I&EC research
Industrial & Engineering Chemistry Research

pubs.acs.org/IECR
Article

Natural Gas Well Production Network State-Space Model Development and Validation for Process Control

Rudzani Dzedzemane, Andries Johannes Wiid, Johan Derik le Roux,* and Ian Keith Craig

Cite This: *Ind. Eng. Chem. Res.* 2024, 63, 1461−1473

ABSTRACT: A transient state-space nonlinear model is developed for a natural gas system fed from multiple gas wellheads. The dynamic models are developed by making use of the spectral element method for pipeline spatial discretization. Wellhead models are integrated into the pipeline models by making use of suitable boundary conditions based on the characteristic compatibility method. The models are validated against a large scale natural gas well production network. The validation shows that the model has a good prediction performance based on a low normalized root-mean-square error of at most 5.08% and a high Pearson correlation coefficient with measured plant data of at least 0.94. The good prediction response of the developed transient models makes them suitable for use in model-based optimal control of natural gas well production networks. The resulting dynamic model can be easily adapted to a gas network of any configuration due to its modular form.

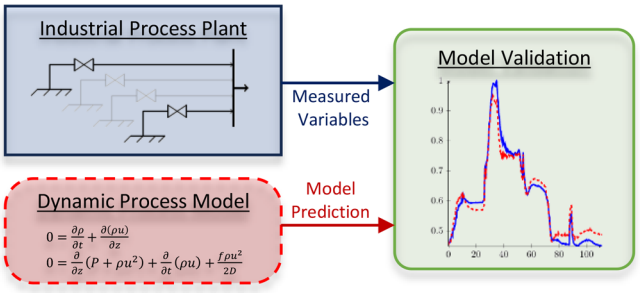

INTRODUCTION

Natural gas is an energy source that has a higher efficiency compared to coal and oil. It also releases less harmful products when burnt.[1] Therefore, it has the potential to play an important role in the decarbonization of a coal based economies such as South Africa, Poland, India, and China where 90%,[2] 72%,[3] 71%,[3] and 60%,[4] respectively, of electricity is generated from coal. The importance of using natural gas as an intermediary energy source has been recognized by the industrial sector which aims to use natural gas in its transition to net-zero emissions.[5,6]

The main control objectives in a natural gas supply and distribution network are meeting consumer gas demand while maintaining the supply header pressure within predefined operating limits. If the customer demand is not met, then the header pressure will reduce below a low specification limit and affect the performance of customer equipment, such as gas fired heaters. If the header pressure increases above a safe limit, then safety systems will trip the supply of gas from the natural gas wells, resulting in financial losses. Constraints on the flow rate of gas from natural gas wells result in an additional control requirement. A flow rate that is too high can result in water coning and delivering an undesired amount of water to the processing facility.[7] A low flow rate can result in liquid loading, which occurs when the gas velocity is too low to carry condensate or liquids with the gas stream. The liquid was allowed to accumulate in the wellbore. If the accumulation problem is not rectified, then production from the well may stop, and the well will be abandoned.[8] Therefore, the flow rate from each well has to be controlled between the predefined low and high flow limits.

A natural gas well production network is typically a multiple-input, multiple-output (MIMO) system with multiple wells feeding a header that supplies multiple consumers. The production network is highly interactive as a change in a single gas flow from one well affects the network pressure, thereby affecting the flow of gas from all other wells in the network simultaneously, as flow controllers are not acting on the valves to maintain a constant flow. The constraint on the gas flows from the wells makes this a constrained MIMO system that can be effectively controlled using a model based control method such as model predictive control (MPC).[9] Since MPC requires a dynamic model of the process to be controlled, this paper investigates the development of such a model for a natural gas well production network. The resulting model is in a form that is suitable for process control applications and validated by using industrial process data.

The natural gas system model consists of a model of the deliverability of each gas well[1,10] and a model of the natural gas pipeline network. Various authors have considered steady-state

Received: March 27, 2023
Revised: September 18, 2023
Accepted: December 8, 2023
Published: January 11, 2024

https://doi.org/10.1021/acs.iecr.3c00990
Ind. Eng. Chem. Res. 2024, 63, 1461−1473

models of gas pipeline networks for the purposes of steady-state optimization.[11−14] Such models are suitable for production planning purposes but cannot be used for control applications as they do not capture the transient behavior of the gas network. Considerable work has been done on developing transient models of gas pipeline networks. The transient models are composed of hyperbolic partial differential equations, which increases the complexity of the model development problem. The hyperbolic partial differential equations can be solved for the network pressure and flow transients by making use of finite difference methods,[15−17] finite volume methods (FVM),[18] finite element methods (FEM),[19,20] the method of characteristics (MOC),[18,21] and spectral element methods (SEM).[22−24]

Su et al.[25] developed a linearized transient model of a pipeline network by making use of the finite difference method for spatial discretization. The resulting model accuracy was evaluated by comparing its performance against those of previous models and simulation software. The linearization, however, can result in model errors that can negatively affect the performance of model based controllers during large disturbance conditions. A numerically stable method of treating boundary conditions was also not included in the study. Kessal[17] made use of an explicit finite difference method for time and spatial discretization in order to model slow transients in a gas pipeline. Chaczykowski and Zarodkiewicz[15] developed a pipe network model by making use of an implicit finite difference method in both time and space. Koo[18] made use of an implicit finite volume method and an implicit MOC approach to solve the hyperbolic differential equations. However, implicit methods are not ideal for model based control applications due to the time required to recursively solve the resulting difference equations. Bermúdez and Shabani[19] make use of FEM to model a gas pipeline network. This method has advantages over finite difference methods as it has a higher accuracy and allows for the use of larger step spatial and time discretization steps while maintaining numerical stability.[19]

The SEM combines the versatility of finite difference methods and the accuracy of the FEM by implementing a spectral method on a spatially discretized section of the pipeline. The work in Mennemann et al.[23] made use of the SEM to develop a dynamic model of a pipeline for an incompressible fluid while the work in Wiid et al.[24] extended this model to a compressible fluid with non-constant values for the compressibility factor, molecular weight, gas viscosity, and pipe friction factor. This method is ideal for use in control applications as it results in an explicit state-space model that can be solved with low computational complexity.[23] By way of example, an industrial gas pipeline plant is modeled and validated by Wiid et al.,[24] and the subsequent model is used as part of a model based control strategy.[26]

This paper extends on the work in Wiid et al.[24] to include a model of the natural gas wells feeding the pipeline. The dynamic model is validated against online industrial plant data.[24,27−31] The novelty in this study is the implementation of SEM to a large number of interconnected pipelines and the subsequent development of suitable boundary conditions for gas wells, choke valves, and consumers with the aim of obtaining an overall numerically stable gas network model.

SINGLE GAS PIPELINE DYNAMIC MODEL DEVELOPMENT

This section presents the governing equations for gas flow in a single pipeline and provides definitions of the natural gas properties required in the models. The nomenclature used in the model development is given in Table 1.

Table 1. Nomenclature

symbol	description	units
A	Pipe cross sectional area	m^2
C_v	Choke valve flow coefficient	
C_w	Well deliverability coefficient	
D	Pipe internal diameter	m
f	Pipe friction factor	
l	Choke valve open command	
L	Pipe length	m
M_w	Gas molar weight	kg/mol
P	Pressure	Pa
P_C	Critical pressure	Pa
P_e	Reservoir pressure	Pa
P_{TH}	Well tubing head pressure	Pa
q	Gas flow rate	kg/s
R	Gas constant	m^3 Pa $Kmol^{-1}$
Re	Reynolds number	
T	Temperature	K
T_C	Critical temperature	K
u	Gas velocity	m/s
Z	Gas compressibility factor	
ρ	Gas density	kg/m^3
ρ_C	Critical gas density	kg/m^3
η	Gas viscosity	Pa.s
ϵ	Pipe roughness	m

Single Pipeline Gas Flow Governing Equations. Gas flow dynamics in a gas pipeline is governed by a continuity (eq 1) and momentum (eq 2).[32] These equations are

$$0=\frac{\partial \rho}{\partial t}+\frac{\partial(\rho u)}{\partial z} \tag{1}$$

$$0=\frac{\partial P}{\partial z}+\frac{\partial(\rho u)}{\partial t}+\frac{\partial(\rho u^2)}{\partial z}+\frac{f\rho u^2}{2D} \tag{2}$$

where ρ is the gas density, P is the gas pressure, u is the gas velocity, t is the time instant, z is the position along the pipeline, and f is the pipe friction factor. Equations 1 and 2 can be converted into equations based on mass flow rate and pressure instead of density and velocity. This conversion is required because online density measurements for gas streams are not readily available in process plants. The conversion is based on the ideal gas (eq 3) and the velocity to mass flow rate conversion (eq 4). These equations are

$$PM_w = \rho ZRT \tag{3}$$

$$q = A\rho u \tag{4}$$

The continuity and momentum equations with mass flow rate and pressure as the conserved variables are

$$0 = \frac{\partial P}{\partial t}+\frac{c^2}{A}\frac{\partial q}{\partial z} \tag{5}$$

https://doi.org/10.1021/acs.iecr.3c00990
Ind. Eng. Chem. Res. 2024, 63, 1461−1473

$$0 = \frac{\partial q}{\partial t} + A\frac{\partial P}{\partial z} + \frac{fc^2}{2AD}\frac{q^2}{P} \tag{6}$$

where

$$c = \sqrt{\frac{ZRT}{M_w}} \tag{7}$$

is the speed of sound in the gas medium.

The third term in the momentum in eq 2 is assumed to be negligible when converting eq 2 to eq 6. This assumption is valid because the gas flow velocities are much lower than the speed of sound c.[32] The gas temperature T is assumed constant along the pipeline as the gas pipes are buried and insulated pipelines with a small difference of at most 20 °C between the gas and ambient temperature. In addition, there are no compressors in the network, which could result in temperature changes. It should be noted that eqs 5 and 6 are only applicable for gas flow in one direction and do not account for reverse flow. However, the one directional flow model is valid as the network being considered in the study is a production network, where reverse flow is prevented in the system design even under abnormal conditions.

Spatial Discretization Using Spectral Element Method. *Weak Formulation of the Pipeline Model.* SEM is used to discretize each pipeline in the network. It is applied by first writing eqs 1 and 2 in conservative matrix form as

$$0 = \frac{\partial}{\partial t}\begin{bmatrix} P \\ q \end{bmatrix} + \begin{bmatrix} 0 & \frac{c^2}{A} \\ A & 0 \end{bmatrix}\frac{\partial}{\partial z}\begin{bmatrix} P \\ q \end{bmatrix} + \begin{bmatrix} 0 \\ \frac{fc^2}{2AD}\frac{q^2}{P} \end{bmatrix} \tag{8}$$

Equation 8 can be converted into the form

$$0 = \frac{\partial}{\partial t}\begin{bmatrix} \epsilon P \\ \mu q \end{bmatrix} + \frac{\partial}{\partial z}\left(\begin{bmatrix} 0 & \frac{1}{\mu} \\ \frac{1}{\epsilon} & 0 \end{bmatrix}\begin{bmatrix} \epsilon P \\ \mu q \end{bmatrix}\right) + \begin{bmatrix} 0 \\ r\Theta(P, q) \end{bmatrix} \tag{9}$$

where $\epsilon = \frac{A}{c^2}$, $\mu = \frac{1}{A}$, $r = \frac{\mu f c^2}{2AD}$, and $\Theta(P, q) = \frac{q^2}{P}$.

SEM makes use of a weak formulation of the differential equation shown in eq 9, which is used to calculate an estimate of the spatial solution. A class of test functions v are chosen in order to implement the estimate as an integral of weighted residuals.[33] Therefore, the weak formulation is implemented by multiplying eq 9 by the test functions v and then integrating over the spatial domain $[0, L]$. The weak formulation is given by[23]

$$\int_0^L \left(\frac{\partial}{\partial t}\begin{bmatrix} \epsilon P \\ \mu q \end{bmatrix} + \frac{\partial}{\partial z}\left(\begin{bmatrix} 0 & \frac{1}{\mu} \\ \frac{1}{\epsilon} & 0 \end{bmatrix}\begin{bmatrix} \epsilon P \\ \mu q \end{bmatrix}\right) + \begin{bmatrix} 0 \\ r\Theta \end{bmatrix}\right) v \, dz = 0 \tag{10}$$

Applying integration by parts on eq 10 results in

$$\int_0^L \frac{\partial}{\partial t}\begin{bmatrix} \epsilon P \\ \mu q \end{bmatrix} v \, dz = \int_0^L \begin{bmatrix} q \\ P \end{bmatrix}\frac{\partial v}{\partial z} \, dz - \int_0^L r\begin{bmatrix} 0 \\ \Theta \end{bmatrix} v \, dz + \boldsymbol{F}^*(0, t)v(0) - \boldsymbol{F}^*(L, t)v(L) \tag{11}$$

where $\boldsymbol{F}^*(z, t) = [\boldsymbol{F}_1^*(z, t), \boldsymbol{F}_2^*(z, t)]^T$ is the flux evaluated at spatial location z and time t.

Spatial Discretization. The spatial domain $\Omega = [0, L]$ is divided into M elements Z_m such that

$$\Omega = \bigcup_{m=1}^{M} Z_m \tag{12}$$

where $Z_m = [\overline{z}_{m-1}, \overline{z}_m]$ for $m = 1, 2, ..., M-1, M$. The element edges satisfy $\overline{z}_0 = 0 < \overline{z}_1 < ... < \overline{z}_{M-1} < \overline{z}_M = L$.[23] The spectral method is applied to solve the integrals in eq 11 by approximating the solution as a sum of elemental basis functions.

Elemental Basis Functions. The spectral method makes use of the characteristic Lagrange polynomials as elemental basis functions. The characteristic Lagrange polynomials of degree N_m in the reference domain $\hat{\Omega} = [-1, 1]$ are given by[22]

$$\varphi_i^{(m)}(\varepsilon) = \frac{\frac{\lambda_i}{\varepsilon - \varepsilon_i}}{\sum_{k=0}^{N_m}\frac{\lambda_k}{\varepsilon - \varepsilon_k}} \tag{13}$$

where

$$\lambda_i = \frac{1}{\prod_{k\neq i}(\varepsilon_i - \varepsilon_k)} \tag{14}$$

for $i = 0, 1, ..., N_m$ and $\varepsilon \in \hat{\Omega}$. The form of the characteristic Lagrange polynomials in eq 13 is called the Barycentric form and is more numerically stable as compared to the standard form.[22] The points or nodes $\varepsilon_0, \varepsilon_1, ..., \varepsilon_{N_m}$ are the Legendre−Gauss−Lobatto (LGL) nodes and are calculated as the zeros of $(1 - \varepsilon^2)P'_{N_m}$ where P_{N_m} is the characteristic Legendre polynomial of order N_m and P'_{N_m} is the first derivative of the characteristic Legendre polynomial with respect to ε.

The elemental basis functions can be mapped from the reference domain $\hat{\Omega}$ to the spatial element domain by making use of the transform

$$\Gamma_m(\varepsilon) = z_m = \frac{\overline{z}_m - \overline{z}_{m-1}}{2}\varepsilon + \frac{\overline{z}_m + \overline{z}_{m-1}}{2} \tag{15}$$

The transformation in eq 15 is used to define the elemental basis function in the spatial domain $z \in [\overline{z}_{m-1}, \overline{z}_m]$ as[22,23]

$$\varphi_i^m(z) = \varphi_i^m(\Gamma_m^{-1}(z)) \tag{16}$$

Global Basis Functions. The element basis functions are combined to create global basis functions $\phi_j(z)$ which are continuous over the spatial interval $z \in [0, L]$ for $j = 1, 2, ... \sum N_m + 1$. Element basis function i in element m corresponds to global basis function $j = (N_m - 1)(m - 1) + i$. In forming global basis function j, element basis function i in domain m is extended to cover the domain of the global basis function as described below

$$\phi_j(z) = \begin{cases} \varphi_i^m(z) & \text{for } z \in Z_m \\ 0 & \text{otherwise} \end{cases} \tag{17}$$

Special consideration has to be taken for the case when $i = 0$ and $i = N_m$ in order to ensure that the global basis function is smooth. The element basis functions for these cases are converted into global basis functions by joining element basis functions φ_0^{m+1} and $\varphi_{N_m}^m$ as[22]

https://doi.org/10.1021/acs.iecr.3c00990
Ind. Eng. Chem. Res. 2024, 63, 1461−1473

$$\phi_j(z) = \begin{cases} \varphi_{N_m}^m(z) & \text{for } z \in Z_m \\ \varphi_0^m(z) & \text{for } z \in Z_{m+1} \\ 0 & \text{otherwise} \end{cases} \tag{18}$$

Solution Approximation using Global Basis Functions. A polynomial approximation of the solution of eq 11 based on the global basis functions defined earlier is given by

$$P(z, t) \approx P_h(z, t) = \sum_{j=1}^{J} P_j(t)\phi_j(z) \tag{19}$$

$$q(z, t) \approx q_h(z, t) = \sum_{j=1}^{J} q_j(t)\phi_j(z) \tag{20}$$

The nonlinear term $\Theta(P, q)$ in eq 9 is approximated as

$$\Theta(z, t) \approx \Theta_h(z, t) = \sum_{j=1}^{J} \Theta_j(t)\phi_j(z) \tag{21}$$

Weak Formulation Solution. The SEM used in this study is a Galerkin method. This is a spectral method in which the form of the basis functions are the same as the test functions.[33] Therefore, the test functions are given by $\phi_i(z)$.

The weak formulation in eq 11 is solved by substituting the polynomial approximations of $P(z, t)$, $q(z, t)$, and $\Theta(z, t)$ into eq 11. $\phi_i(z)$ is substituted in place of the test functions. The weak formulation for eq 11 is therefore

$$\begin{aligned} &\frac{\partial P_1(t)}{\partial t}\int_0^L \epsilon\phi_1(z)\phi_i(z)\,dz + \ldots + \frac{\partial P_J(t)}{\partial t}\int_0^L \epsilon\phi_J(z)\phi_i(z)\,dz \\ &= q_1(t)\int_0^L \phi_1(z)\frac{\partial\phi_i(z)}{\partial z}\,dz + \ldots + q_J(t) \\ &\int_0^L \phi_J(z)\frac{\partial\phi_i(z)}{\partial z}\,dz + q^*(0, t)\phi_i(0) - q^*(L, t)\phi_i(L) \end{aligned} \tag{22}$$

and

$$\begin{aligned} &\frac{\partial q_1(t)}{\partial t}\int_0^L \mu\phi_1(z)\phi_i(z)\,dz + \ldots + \frac{\partial q_J(t)}{\partial t} \\ &\int_0^L \mu\phi_J(z)\phi_i(z)\,dz = P_1(t)\int_0^L \phi_1(z)\frac{\partial\phi_i(z)}{\partial z}\,dz \\ &+ \ldots + P_J(t)\int_0^L \phi_J(z)\frac{\partial\phi_i(z)}{\partial z}\,dz \\ &- \left[\Theta_1(t)\int_0^L r\phi_1(z)\phi_i(z)\,dz + \ldots + \Theta_J(t)\right. \\ &\left.\int_0^L r\phi_J(z)\phi_i(z)\,dz\right] + P^*(0, t)\phi_i(0) - P^*(L, t)\phi_i(L) \end{aligned} \tag{23}$$

Equations 22 and 23 can be written in matrix form by defining

$$S_{i,j} = \int_0^L \phi_j(z)\frac{\partial\phi_i(z)}{\partial z}\,dz \tag{24}$$

$$(M_x)_{i,j} = \int_0^L x(z)\phi_j(z)\phi_i(z)\,dz \tag{25}$$

where $S_{i,j}$ is the stiffness matrix value for test function i and node j, and $(M_x)_{i,j}$ is the mass matrix value for test function i and node j. The row position in the matrices is i and the column position is j. The resulting matrix form of the weak formulation solution is[23]

$$\boldsymbol{M}_c\frac{\partial \mathbf{P}}{\partial t} = \boldsymbol{S}\boldsymbol{q} + \boldsymbol{q}_1^*\mathbf{e_1} - \boldsymbol{q}_J^*\mathbf{e_J} \tag{26}$$

$$\boldsymbol{M}_\mu\frac{\partial \boldsymbol{q}}{\partial t} = \mathbf{S}\mathbf{P} - \boldsymbol{M}_r\boldsymbol{\Theta} + \boldsymbol{P}_1^*\mathbf{e_1} - \boldsymbol{P}_J^*\mathbf{e_J} \tag{27}$$

where $\boldsymbol{P} = [\boldsymbol{P}_1, \boldsymbol{P}_2, \ldots, \boldsymbol{P}_J]^T$, $\boldsymbol{q} = [\boldsymbol{q}_1, \boldsymbol{q}_2, \ldots, \boldsymbol{q}_J]^T$, $\Theta = [\Theta_1, \Theta_2, \ldots, \Theta_J]^T$, $\mathbf{e_1} = [1, 0, 0, 0, \ldots, 0]^T$ and $\mathbf{e_J} = [0, 0, \ldots, 1]^T$.

Mass and Stiffness Matrix Calculation. The solution of the mass and stiffness matrices is based on the quadrature formula of Canuto et al.,[33] such that

$$\int_{-1}^{1} p(\varepsilon)\,d\varepsilon = \sum_{j=0}^{N_m} p(\varepsilon_j)w_j \tag{28}$$

where w_j is the integration weight. For the LGL nodes, the integration weights are calculated by

$$w_j = \frac{2}{N_m(N_m + 1)[P_{N_m}(\varepsilon_j)]^2} \tag{29}$$

The quadrature formula can be transformed from the reference domain $\hat{\Omega}$ to the spatial domain by making use of transform eq 15. The resulting quadrature formula is

$$\int_{\bar{z}_{m-1}}^{\bar{z}_m} p(z)\,dz = \frac{h}{2}\sum_{j=0}^{N_m} p(z)w_j \tag{30}$$

where $h = \bar{z}_m - \bar{z}_{m-1}$. The same spatial discretization length (h) is assumed in each element. Therefore, the elements of the mass and stiffness matrices are

$$\begin{aligned} (M_x)_{i,j} &= \int_0^L x(z)\phi_j(z)\phi_i(z)\,dz \\ &= \frac{h}{2}\sum_{k=1}^{J} x(z_k)\phi_j(z_k)\phi_i(z_k)w_k \\ &= \begin{cases} \frac{h}{2}x(z_i)w_i & \text{for } i = j = k \\ 0 & \text{otherwise} \end{cases} \end{aligned} \tag{31}$$

$$\begin{aligned} S_{i,j} &= \int_0^L \phi_j(z)\frac{\partial\phi_i(z)}{\partial z}\,dz \\ &= \sum_{k=1}^{J} \phi_j(z_k)\frac{\partial\phi_i(z_k)}{\partial z}w_k \\ &= \frac{\partial\phi_i(z_j)}{\partial z}w_j \end{aligned} \tag{32}$$

The derivative of the test function in eq 32 is calculated by[22]

$$\frac{\partial\phi_i(z_k)}{\partial z} = \sum_{l=0}^{N} (D_N)_{k,l}\phi_i(z_l) = (D_N)_{j,i}w_j \tag{33}$$

where

https://doi.org/10.1021/acs.iecr.3c00990
Ind. Eng. Chem. Res. 2024, 63, 1461−1473

$$(D_N)_{k,l} = \begin{cases} \dfrac{P_N(z_k)}{P_N(z_l)}\dfrac{1}{z_k - z_l} & \text{for } k \neq l \\ \dfrac{-(N+1)N}{4} & \text{for } k = l = 0 \\ \dfrac{N(N+1)}{4} & \text{for } k = l = N \\ 0 & \text{otherwise} \end{cases} \tag{34}$$

Boundary Conditions. The choice of boundary conditions for the hyperbolic system shown in eq 9 can have a large influence on the stability of the solution. A stable method of enforcing boundary conditions is the characteristic compatibility method (CCM).[22] The CCM method is implemented by first writing eq 9 in compact form as

$$\frac{\partial \mathbf{U}}{\partial t} + \mathbf{A}\frac{\partial \mathbf{U}}{\partial z} + f(\mathbf{U}) = 0 \tag{35}$$

where $\mathbf{U}$ is a vector containing the physical variables of flow rate and pressure. $\mathbf{U}$ is converted into characteristic variables $\mathbf{Z}$ that travels in only one wave direction by

$$\mathbf{Z}=\mathbf{W}^{-1}\mathbf{U} \tag{36}$$

where $\mathbf{W}$ is the eigenvector matrix of parameter $\mathbf{A}$ in eq 35.

The CCM method is implemented at each boundary by expressing the incoming characteristic variables at the boundary in terms of the outgoing characteristic variables and boundary data. Variables used in the boundary condition calculations are listed in Figure 1. The boundary condition at

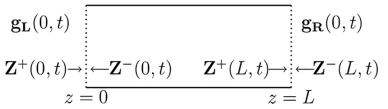

Figure 1. Variables used in calculating boundary conditions where the left-hand side is the inlet and the right-hand side is the outlet of the pipe.

the pipe inlet ($z = 0$) is given by $\mathbf{g}_L(0, t)$ and the boundary condition at the pipe outlet ($z = L$) is given by $\mathbf{g}_R(L, t)$. $\mathbf{Z}^-(0, t)$ is the characteristic variable propagated from the pipe interior toward the pipe inlet boundary, while $\mathbf{Z}^+(0, t)$ is the characteristic variable propagated from the inlet boundary toward the pipe interior. $\mathbf{Z}^-(L, t)$ is the characteristic variable propagated from the pipe outlet boundary toward the pipe interior, while $\mathbf{Z}^+(L, t)$ is the characteristic variable propagated from the pipe interior toward the pipe outlet boundary.

Boundary Condition Implementation at Pipe Inlet. Boundary conditions at the pipe inlet are written in terms of the physical and characteristic variables as

$$\mathbf{B}_L\mathbf{U}(0, t) = \mathbf{g}_L(0, t) \tag{37}$$

$$\mathbf{C}_L\mathbf{Z}(0, t) = \mathbf{g}_L(0, t) \tag{38}$$

$$\mathbf{C}_L{}^+\mathbf{Z}^+(0, t) + \mathbf{C}_L{}^-\mathbf{Z}^-(0, t) = \mathbf{g}_L(0, t) \tag{39}$$

where

$$\mathbf{C}_L = \mathbf{B}_L\mathbf{W}_L \tag{40}$$

and $\mathbf{B}_L$ is a matrix that relates the boundary constraint $\mathbf{g}_L(0, t)$ to the physical variables $\mathbf{U}$. The expression for the incoming characteristic ($\mathbf{Z}^+$) at the inlet boundary can be derived from eq 39 resulting in

$$\mathbf{Z}^+(0, t) = \mathbf{S}_L\mathbf{Z}^-(0, t) + \mathbf{Z}_L(t) \tag{41}$$

where

$$\mathbf{S}_L=-(\mathbf{C}_L{}^+)^{-1}(\mathbf{C}_L)^- \tag{42}$$

$$\mathbf{Z}_L(t) = (\mathbf{C}_L{}^+)^{-1}\mathbf{g}_L(t) \tag{43}$$

Since $\mathbf{Z}^-(0, t)$ is the characteristic variable that is propagated from the interior, it can be expressed as

$$\mathbf{Z}^-(0, t) = (\mathbf{W}^-)^{-1}\begin{bmatrix} P_1 \\ q_1 \end{bmatrix} \tag{44}$$

Boundary Condition Implementation at Pipe Outlet. Boundary conditions at the pipe outlet are written in terms of the physical and characteristic variables as

$$\mathbf{B}_R\mathbf{U}(L, t) = \mathbf{g}_R(L, t) \tag{45}$$

$$\mathbf{C}_R\mathbf{Z}(L, t) = \mathbf{g}_R(L, t) \tag{46}$$

$$\mathbf{C}_R{}^+\mathbf{Z}^+(L, t) + \mathbf{C}_R{}^-\mathbf{Z}^-(L, t) = \mathbf{g}_R(L, t) \tag{47}$$

where

$$\mathbf{C}_R = \mathbf{B}_R\mathbf{W}_R \tag{48}$$

and $\mathbf{B}_R$ is a matrix that relates the boundary constraint $\mathbf{g}_R(L, t)$ to the physical variables $\mathbf{U}$.

The expression for the incoming characteristic ($\mathbf{Z}^-$) at the outlet boundary is given by

$$\mathbf{Z}^-(L, t) = \mathbf{S}_R\mathbf{Z}^+(L, t) + \mathbf{Z}_R(t) \tag{49}$$

where

$$\mathbf{S}_R=-(\mathbf{C}_R{}^-)^{-1}(\mathbf{C}_R)^+ \tag{50}$$

$$\mathbf{Z}_R(t) = (\mathbf{C}_R{}^-)^{-1}\mathbf{g}_R(t) \tag{51}$$

Since $\mathbf{Z}^+(L, t)$ is the characteristic variable that is propagated from the interior, it can be expressed as

$$\mathbf{Z}^+(L, t) = (\mathbf{W}^+)^{-1}\begin{bmatrix} P_J \\ q_J \end{bmatrix} \tag{52}$$

Application of the CCM Method to Calculate Boundary Conditions. The CCM method is used to calculate the values of $\mathbf{F}^*(0, t)$ and $\mathbf{F}^*(L, t)$ in eq 11 as shown below.

$$\begin{aligned}\mathbf{F}^*(0, t) &= \mathbf{A}\mathbf{U}(0, t) = \mathbf{W}\mathbf{\Lambda}\mathbf{Z}(0, t) \\ &= \mathbf{W}^+\mathbf{\Lambda}^+\mathbf{Z}^+(0, t) + \mathbf{W}^-\mathbf{\Lambda}^-\mathbf{Z}^-(0, t)\end{aligned} \tag{53}$$

$$\begin{aligned}\mathbf{F}^*(L, t) &= \mathbf{A}\mathbf{U}(L, t) = \mathbf{W}\mathbf{\Lambda}\mathbf{Z}(L, t) \\ &= \mathbf{W}^+\mathbf{\Lambda}^+\mathbf{Z}^+(L, t) + \mathbf{W}^-\mathbf{\Lambda}^-\mathbf{Z}^-(L, t)\end{aligned} \tag{54}$$

The expression for the incoming characteristic at the inlet boundary is substituted into eq 53 resulting in

$$\mathbf{F}^*(0, t) = (\mathbf{W}^+\mathbf{\Lambda}^+\mathbf{S}_L + \mathbf{W}^-\mathbf{\Lambda}^-)\mathbf{Z}^-(0, t) + \mathbf{W}^+\mathbf{\Lambda}^+\mathbf{Z}_L(t) \tag{55}$$

Similarly, the expression for the incoming characteristic at the outlet boundary is substituted into eq 54 resulting in

https://doi.org/10.1021/acs.iecr.3c00990
Ind. Eng. Chem. Res. 2024, 63, 1461−1473

$$\mathbf{F}^{*}(L, t) = (\mathbf{W}^{+}\mathbf{\Lambda}^{+} + \mathbf{W}^{-}\mathbf{\Lambda}^{-}\mathbf{S}_{\mathbf{R}})\mathbf{Z}^{+}(L, t) + \mathbf{W}^{-}\mathbf{\Lambda}^{-}\mathbf{Z}_{\mathbf{R}}(t) \tag{56}$$

where $\mathbf{Z}^{-}(0, t)$ and $\mathbf{Z}^{+}(L, t)$ are given by eqs 44 and 52, respectively.

Estimation of Single Pipeline Model Unknown Parameters. The unknown parameters in the single pipeline model are the gas compressibility factor (Z) and the pipeline friction factor (f). The pipeline model parameters are calculated from first-principles using the equations described in this section. The gas molar weight (M_w) is assumed to be constant and is known over the entire gas field. It should be noted that the developed model is independent of the network operating conditions due to all pipeline model parameters being calculated from first-principles instead of being estimated from operating data.

Gas Compressibility Factor. The compressibility factor (Z) is calculated by making use of the following explicit correlation[34,35]

$$Z = \frac{DP_{Pr}(1 + Y + Y^2 - Y^3)}{(DP_{Pr} + EY^2 - FY^{G})(1 - Y)^3} \tag{57}$$

where

$$Y = \frac{DP_{Pr}}{\frac{a + A^2}{C} - \frac{A^2 B}{C^3}}$$

Parameters A, B, C, D, E, F, and G are functions of the pseudo-reduced temperature and pressure. Expressions for these parameters can be found in Kareem et al.[35]

The pseudo-reduced pressure (P_{Pr}) and temperature (T_{Pr}) in eq 57 are given by $P_{Pr} = \frac{P}{P_C}$ and $T_{Pr} = \frac{T}{T_C}$ where P_C is the pseudo-critical pressure and T_C is the pseudo-critical temperature. The pseudo-critical temperature and pressures are calculated based knowledge of the gas composition. P_C is given by

$$P_C = \sum_i y_i P_{Ci} \tag{58}$$

where y_i is the mole fraction of the i-th component in the gas and P_{Ci} is the critical pressure of the i-th component. Similarly T_C is given by

$$T_C = \sum_i y_i T_{Ci} \tag{59}$$

The equation is valid for $0.2 < P_{Pr} < 15$ and $1.15 < T_{Pr} < 3$ and was chosen for its low complexity and low estimation error in this range.

Coefficient of Friction. The friction factor is calculated using correlation[36,37]

$$f = \left(\frac{2.51/Re + 1.1513\delta}{\delta - (\epsilon/D) - 2.3026\delta \log \delta}\right)^2 \tag{60}$$

where

$$\delta = \frac{6.0173}{Re(0.07(\epsilon/D) + Re^{-0.885})^{0.109}} + \frac{\epsilon/D}{3.71} \tag{61}$$

where Re is the Reynolds number and ϵ is the pipe roughness. The Reynolds number is calculated by

$$Re = \frac{\rho u L}{\mu} \tag{62}$$

where μ is the dynamic viscosity and is calculated as

$$\mu = B\sqrt{T_{Pr}}\exp\left(\frac{\theta + (A_b + A_k T_{Pr})\rho_{Pr}^{\alpha}}{T_{Pr}}\right)\sum_{i=1}^{n} y_i\sqrt{M_i} \tag{63}$$

where constants B, θ, A_k, A_b, and α are defined in Yang et al.[38]

The correlation in eq 60 is recommended by Zeghadnia et al.[36] after comparisons with other explicit friction factor coefficient correlation methods.

GAS WELL DELIVERABILITY MODEL

A typical gas well is shown in Figure 2. The gas from the reservoir flows into the well driven by the differential pressure

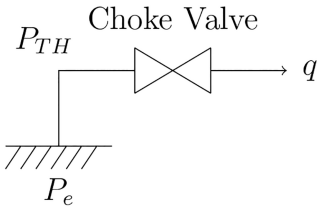

Figure 2. Typical gas well.

between reservoir P_e and pressure in the well outlet P_{TH}. The gas flow can be modeled by,[1,10]

$$q = C_w(P_e^2 - P_{TH}^2)^n \tag{64}$$

where q is the rate of inflow of gas from the reservoir to the wellbore and n is a factor that is used to capture deviation of the well performance from the performance estimated from Darcy's law.[1] This value has to be estimated for each well based on measured data. Parameter C_w is used to capture the pressure drop from the reservoir to the wellbore and is mainly affected by the reservoir permeability.[1]

CHOKE VALVE MODEL

The gas flow from a well is controlled by making use of a choke valve. This is a specialized valve designed for harsh conditions experienced in wellheads. Although detailed nonlinear models of gas flow through choke valves are available,[39,40] a simplified model as defined in ANSI/ISA-75.01.01[41] will be used in this study. This model is given by

$$q = C_v P_{TH}\sqrt{\frac{P_{TH} - P_0}{P_{TH} M_w T_{TH} Z}} \tag{65}$$

where P_0 is the choke valve outlet pressure, Z is the choke valve inlet gas compressibility. The valve coefficient C_v will be approximated as a third order polynomial given by[42]

$$C_v = k_1 l^3 + k_2 l^2 + k_3 l \tag{66}$$

where l is the fractional valve lift command.

NATURAL GAS SUPPLY AND DISTRIBUTION NETWORK DESCRIPTION

The natural gas supply and distribution network that will be considered in this study are shown in Figure 3. This network is made up of 12 natural gas wells that feed into one header. The wells produce gas that is mainly composed of methane

https://doi.org/10.1021/acs.iecr.3c00990
Ind. Eng. Chem. Res. 2024, 63, 1461−1473

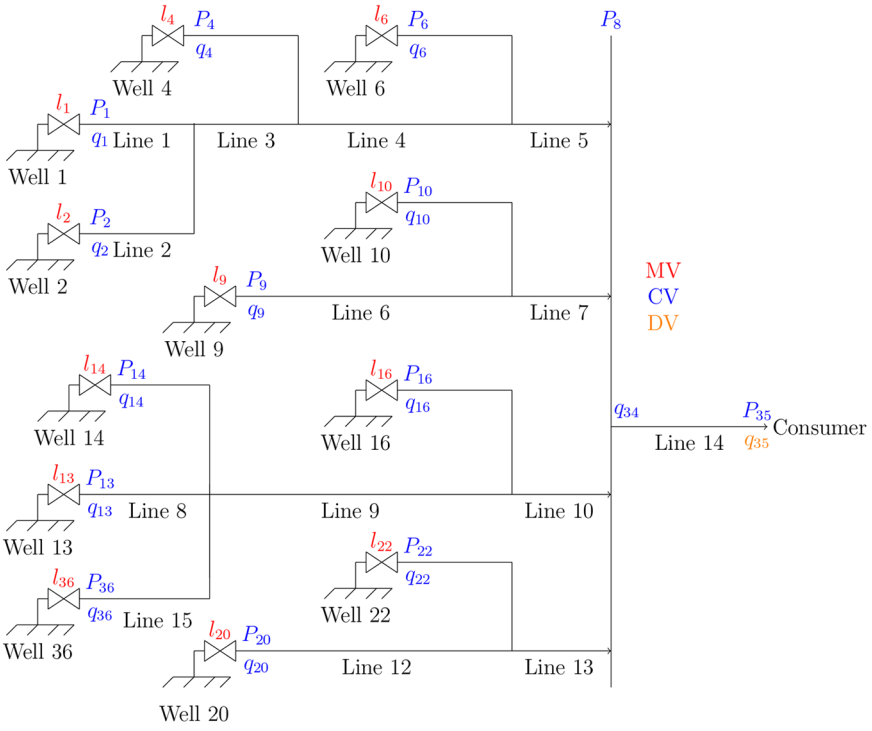

Figure 3. Industrial natural gas supply and distribution network considered in study showing MVs in red, CVs in blue, and DVs in orange. It should be noted that pipelines of negligible length are not assigned line numbers, e.g., pipe from Well 22 to Line 13.

(>90%). The gas compositions in these wells are as shown in Loegering and Milkov[43] for the Pande field. The main control objective in the network is to meet the consumer gas demands. Therefore, the consumer battery limit pressure (P_{35}) is an important controlled variable (CV) as it is an indication of the gas demand (q_{35}) being met. The consumer gas demand (q_{35}) acts as a disturbance variable (DV) for the network. The manipulated variables (MVs) are the choke valve commands (l_i) of each well. The MVs are adjusted in order to set the gas flow rate (q_i) from each well (CVs) in an attempt to meet the gas demands. The network has a high limit on the network pressure (P_8) for safety considerations. This variable is also a CV in the network. All MVs, CVs and DVs in the network are shown in Figure 3.

NATURAL GAS NETWORK MODEL DEVELOPMENT

The gas distribution network model is developed from a state-space model of each pipeline in the network. These models are combined through appropriate junction properties and boundary conditions in order to obtain an overall system state-space model.

Junction Properties Used to Combine Individual Pipeline State-Space Models. The first junction property used to combine individual pipeline models is the assumption that all pressures at a junction are equal:

$$P_{J,i} = P_{1,n} \tag{67}$$

where $P_{J,i}$ is the outlet pressure of the i-th pipeline connected to the junction and $P_{1,n}$ is the inlet pressure of the n-th pipeline connected to the junction.

The second property is the conservation of mass at each junction described by

$$\sum_i q_{J,1} = \sum_n q_{1,n} \tag{68}$$

where $q_{J,i}$ is the outlet flow of the i-th pipeline connected to the junction and $q_{1,n}$ is the inlet flow of the n-th pipeline connected to the junction.

Boundary Conditions for Individual Pipeline Models. Three types of distribution network pipelines are considered in defining pipeline boundary conditions. These are as follow:

- Pipelines connected to a gas well choke valve
- Pipelines connected to a junction
- Pipelines connecting consumers to a header

Applicable boundary conditions for these pipeline types are defined in the sections that follow.

Pipelines Connected to a Gas Well Choke Valve. The boundary conditions for pipelines connected to a gas well through a choke valve are the pipeline inlet pressure $P_0(t)$ and outlet pressure $P_L(t)$. The boundary conditions are therefore defined as

$$\mathbf{B_L U}(0, t) = \mathbf{g_L}(t) = P_0(t) \tag{69}$$

$$\mathbf{B_R U}(0, t) = \mathbf{g_R}(t) = P_L(t) \tag{70}$$

Applying the CCM method to these boundary conditions results in

$$\mathbf{F}^*(0, t) = \begin{bmatrix} q_1^*(t) \\ P_1^*(t) \end{bmatrix} = \begin{bmatrix} q_1(t) + \dfrac{A}{c}(P_0(t) - P_1(t)) \\ P_0(t) \end{bmatrix} \tag{71}$$

https://doi.org/10.1021/acs.iecr.3c00990
Ind. Eng. Chem. Res. 2024, 63, 1461−1473

$$\mathbf{F}^*(L, t) = \begin{bmatrix} q_J^*(t) \\ P_J^*(t) \end{bmatrix} = \begin{bmatrix} q_J(t) + \frac{A}{c}(P_J(t) - P_L(t)) \\ P_L(t) \end{bmatrix} \tag{72}$$

where $P_L(t)$ is an input from the downstream pipeline and $P_0(t)$ is calculated by making use of the gas well deliverability model eq 64 and choke valve model eq 65. Application of eqs 64 and 65 results in the equation for the inlet pressure being given by

$$f(P_0) = 0 = P_e^2 - \left(\frac{q_1^*(t)}{C_w}\right)^{1/n} - P_0(t) \sqrt{P_e^2 - \left(\frac{q_1^*(t)}{C_w}\right)^{1/n}} - a\left(\frac{q_1^*(t)}{C_v}\right)^2 = \sqrt{P_e^2 - \left(\frac{q_1^*(t)}{C_w}\right)^{1/n}} - P_0(t) - \frac{a\left(\frac{q_1^*(t)}{C_v}\right)^2}{\sqrt{P_e^2 - \left(\frac{q_1^*(t)}{C_w}\right)^{1/n}}} \tag{73}$$

where the flux value of flow $q_1^*(t)$ is obtained from eq 71 and is used in the calculation instead of the nodal flow $q_1(t)$ as recommended by Mennemann et al.[23] for improved numerical stability of the model. Equation 73 is solved recursively for the boundary pressure $P_0(t)$.

It can be shown that equation $f(P_0)$ is a monotonically decreasing function by calculating $\frac{\partial f}{\partial P_0}$. Additionally it can be shown that the function result is positive for P_0 given by

$$P_0 = P_1 - \frac{c}{A}q_1$$

It can also be shown that the resulting solution is negative for P_0 given by

$$P_0 = P_1 - \frac{c}{A}q_1 + c_w\frac{c}{A}P_e^{2n_w}$$

These two opposite signed solutions combined with the monotonic nature of the function form numerically convergent initial values for a Newton−Raphson recursive solution.

Pipelines Connected to a Junction. The inlet boundary condition for pipelines connected to a junction is set as the pipe inlet flow rate $q_0(t)$. This flow will be calculated by making use of the conservation of mass at the junction. The outlet boundary condition shall be set as the pipeline outlet pressure which is determined by downstream pipelines. The boundary conditions are therefore defined as

$$\mathbf{B_L}\mathbf{U}(0, t) = \mathbf{g_L}(t) = q_0(t) \tag{74}$$

$$\mathbf{B_R}\mathbf{U}(0, t) = \mathbf{g_R}(t) = P_L(t) \tag{75}$$

Applying the CCM method to these boundary conditions results in

$$\mathbf{F}^*(0, t) = \begin{bmatrix} q_1^*(t) \\ P_1^*(t) \end{bmatrix} = \begin{bmatrix} q_0 \\ P_1 + \frac{c}{A}(q_0 - q_1) \end{bmatrix} \tag{76}$$

$$\mathbf{F}^*(L, t) = \begin{bmatrix} q_J^*(t) \\ P_J^*(t) \end{bmatrix} = \begin{bmatrix} q_J + \frac{A}{c}(P_J - P_L) \\ P_L \end{bmatrix} \tag{77}$$

Pipelines Connecting Consumers to a Header. The inlet boundary condition for pipelines connecting a header to the consumer is set as the inlet flow. This flow was calculated by making use of the conservation of mass at the header. The outlet boundary condition for this pipeline is the demand for the flow from the consumer. Therefore, the boundary conditions are given by

$$\mathbf{B_L}\mathbf{U}(0, t) = \mathbf{g_L}(t) = q_0(t) \tag{78}$$

$$\mathbf{B_R}\mathbf{U}(0, t) = \mathbf{g_R}(t) = q_L(t) \tag{79}$$

Applying the CCM method to these boundary conditions results in

$$\mathbf{F}^*(0, t) = \begin{bmatrix} q_1^*(t) \\ P_1^*(t) \end{bmatrix} = \begin{bmatrix} q_0 \\ P_1 + \frac{c}{A}(q_0 - q_1) \end{bmatrix} \tag{80}$$

$$\mathbf{F}^*(L, t) = \begin{bmatrix} q_J^*(t) \\ P_J^*(t) \end{bmatrix} = \begin{bmatrix} q_L \\ P_J + \frac{c}{A}(q_J - q_L) \end{bmatrix} \tag{81}$$

MODEL PARAMETER ESTIMATION

The unknown model parameters in the gas well deliverability model and choke valve model were estimated from steady-state plant operating data. Due to the nonlinear nature of these models, operating data that represent typical operating conditions have to be used in order to obtain a model that accurately captures the system response around the typical operating conditions.

Well Deliverability Model Parameter Estimation. The unknown parameters in the well deliverability model were obtained by making use of a mean square error estimation method

$$\begin{bmatrix} C_w \\ n \end{bmatrix} = \arg\min_{C_w, n} \frac{1}{N}\sum_{i=0}^{N-1}(q - \hat{q})^2 \tag{82}$$

where $\hat{q}$ is given by eq 64, q is the measured gas flow rate from the well, and N is the total number of measurements. It should be noted that in eq 64 the reservoir pressure P_e is known and assumed constant.

Choke Valve Model Parameter Estimation. The unknown parameters in the choke valve models are also calculated by making use of a mean square error estimator. The estimator used for each well choke valve is given by

$$\begin{bmatrix} k_1 \\ k_2 \\ k_3 \end{bmatrix} = \arg\min_{k_1, k_2, k_3} \frac{1}{N}\sum_{i=0}^{N-1}(q - \hat{q})^2 \tag{83}$$

where $\hat{q}$ is given by eq 65 and q is the measured gas flow rate through the valve.

https://doi.org/10.1021/acs.iecr.3c00990
Ind. Eng. Chem. Res. 2024, 63, 1461−1473

SPECTRAL AND TEMPORAL DISCRETIZATION PARAMETER SETTINGS

Important parameters in the individual pipeline models are the number of spectral elements (M) and the spectral polynomial order (N) for each pipeline. These values determine the spatial discretization length for each pipeline. A constraint is placed on the time discretization step size and spatial discretization length or number of nodes (J) based on the Courant−Friedrichs−Lewy (CFL) condition.[23]

The system under consideration has different length pipelines. The shortest pipe element (pipeline no. 7 in Table 2) was used to determine the time discretization step. For this element, the time discretization was chosen to be 0.5 s, which resulted in a stable model for $N = 2$ and $M = 1$. For all other pipelines, the values of N and M were estimated by increasing them until oscillation errors occurred at a fixed time step size of 0.5 s. The values of N and M obtained using this method are shown in Table 2.

Table 2. Spatial Discretization Settings

pipeline no.	N	M	L (m)
1	2	3	4480
2	2	2	2260
3	2	2	2960
4	2	2	4430
5	2	3	5200
6	3	3	4720
7	2	1	1400
8	3	4	5970
9	2	2	3900
10	2	4	3700
12	2	4	4300
13	3	4	9000
14	6	11	44800
15	2	4	3520

MODEL VALIDATION RESULTS

Plant data was collected for the industrial gas supply and distribution system shown in Figure 3 in order to validate the model developed for the system. Data for modeling and validation was collected over a time period where the system was identified to be at steady-state at time $t = 0$. A steady-state approximation of the models for each pipeline was used to estimate the initial state vectors of the state-space models.

The collected modeling and validation data includes the consumer demand flow rate (q_{35}), consumer battery limit pressure (P_{35}), gas network header pressure (P_8), well tubing head pressures, choke valve outlet pressures, flow rates from each well, and well choke valve command signals. Two modeling data sets were collected. The first data set is steady-state discontinuous data that was manually selected over a period of 8 months in order to develop the steady-state choke valve and steady-state well deliverability models. Periods where the well choke valves were being actuated where selected from the 8 month period and combined to create the steady-state modeling data set. The second modeling data set is dynamic data that was collected over a continuous period of 197 h. The validation data was collected over a continuous period of 120 h and was chosen to be separate from the dynamic and steady-state modeling data periods.

The normalized DV data (q_{35}) used in the model validation, as shown in Figure 4, indicate that the chosen data validation period allows for the evaluation of the model prediction performance in the face of DV changes. The choke valve commands over this period are shown in Figure 5 and relate to the MVs in Figure 3.

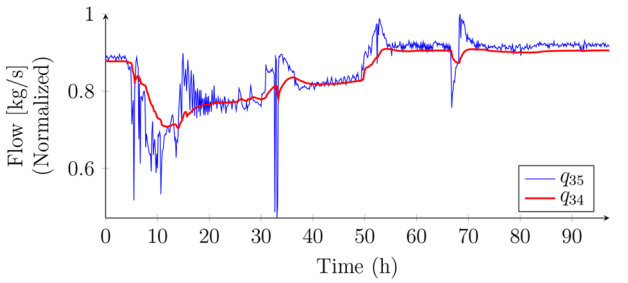

Figure 4. Consumer demand measurements over model validation period.

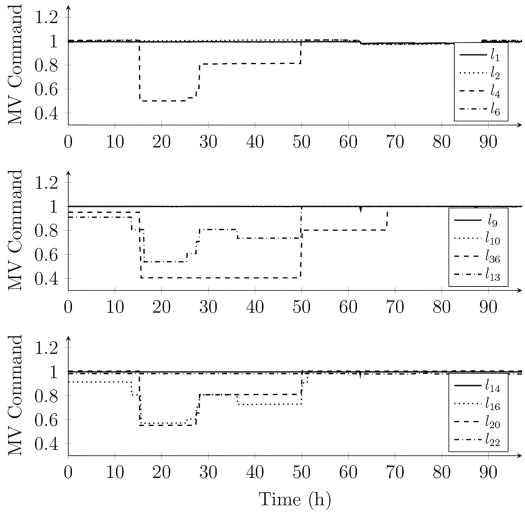

Figure 5. Well choke valve command measurements (normalized) over the model validation period.

The developed model was used to predict the values of all CVs over the validation period as a pure simulation; i.e., no state or parameter updates were performed over the entire simulation period. The model prediction results over the validation data period for the CVs are shown in Figures 6−14. Variables shown in the figures relate to the CVs shown in Figure 3.

Figure 6 shows that the model is able to accurately predict the header pressure and consumer battery limit pressure in the presence of MV and DV changes. The simulation results in Figures 7−10 show that the model can accurately predict the gas supply pressures from each well. The simulation results in Figures 11−14 also show that the developed model can accurately predict the gas flow rates from the wells. Figure 4 demonstrates the ability of the model to accurately capture the system dynamics, as a dynamic lag can be observed between q_{34} and the consumer demand (q_{35}).

Table 3 evaluates the accuracy of the developed models according to the Pearson correlation coefficients ($\rho(y, \hat{y})$) between the plant measurements (y) and model predictions

https://doi.org/10.1021/acs.iecr.3c00990
Ind. Eng. Chem. Res. 2024, 63, 1461−1473

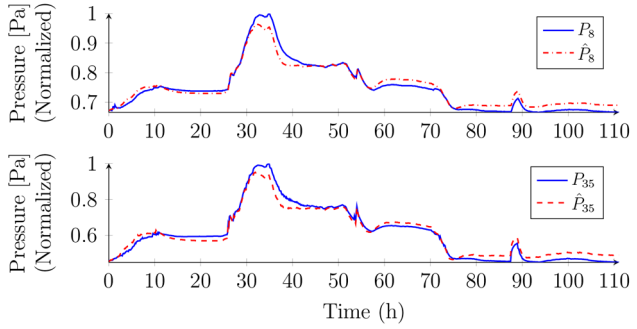

Figure 6. Model validation results for P_8 and P_{35}.

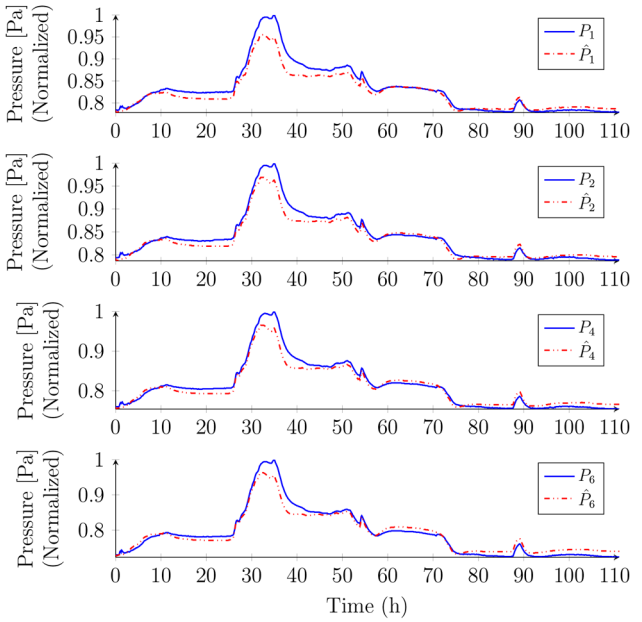

Figure 7. Model validation results for P_1, P_2, P_4 and P_6.

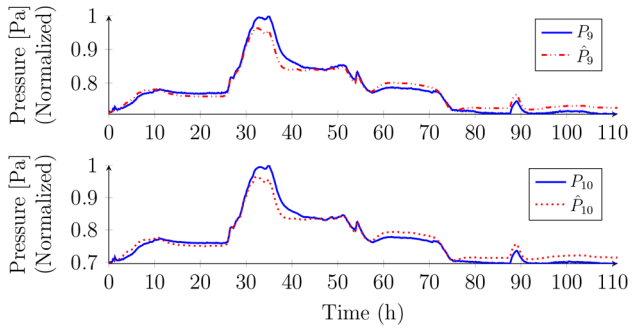

Figure 8. Model validation results P_9 and P_{10}.

($\hat{y}$), as well as the normalized root-mean-square errors (NRMSE) for all CVs. The Pearson correlation coefficients for all CVs are greater than 0.94, which indicates the model is able to accurately capture the directionality of all CV movements. Table 3 shows that the pressure prediction NRMSE is less than 4.35%, while the flow rate prediction NRMSE is less than 5.08%. The low NRMSE values show that the model has good CV prediction performance.

The pressure prediction results in Figures 6−10 show a prediction error at time t = 12 h. This corresponds to a model response to a large change in consumer demand. The pressure

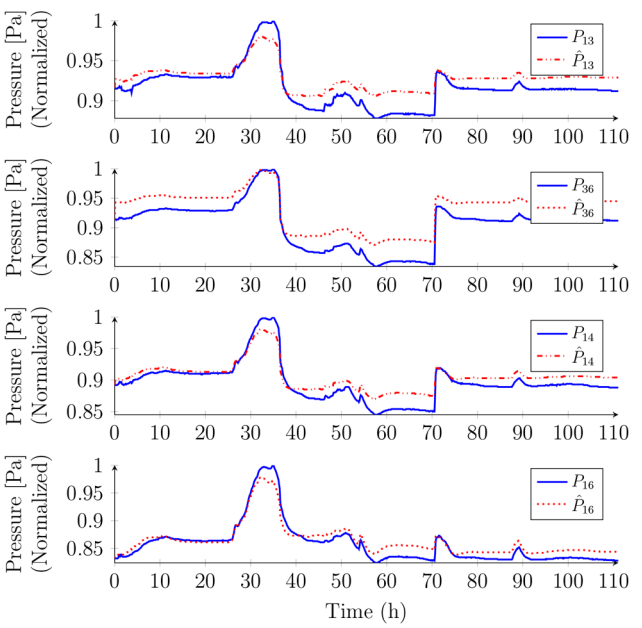

Figure 9. Model validation results P_{13}, P_{36}, P_{14} and P_{16}.

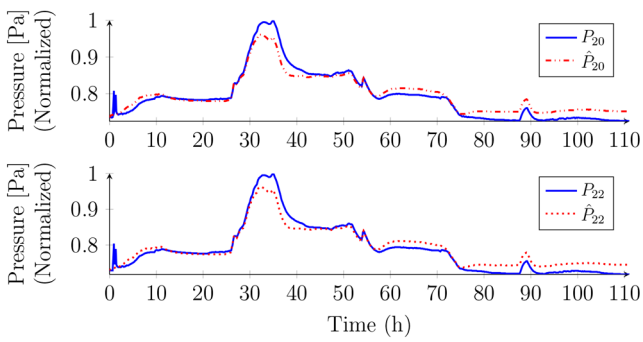

Figure 10. Model validation results for P_{20} and P_{22}.

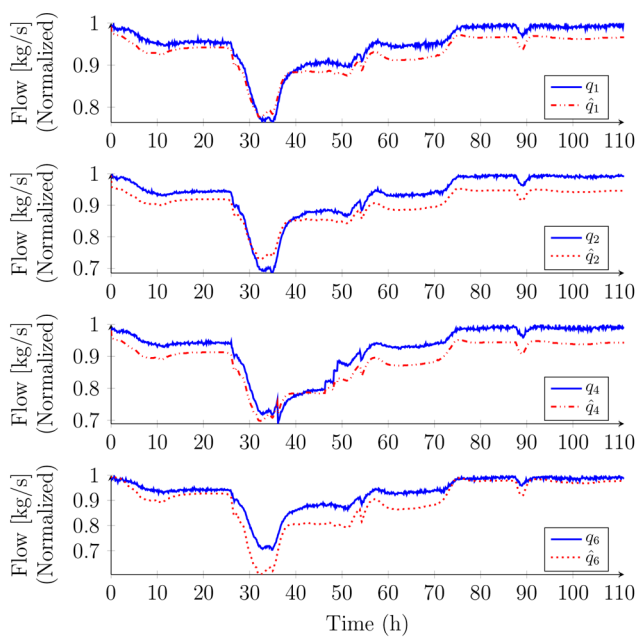

Figure 11. Model validation results for q_1, q_2, q_4 and q_6.

https://doi.org/10.1021/acs.iecr.3c00990
Ind. Eng. Chem. Res. 2024, 63, 1461−1473

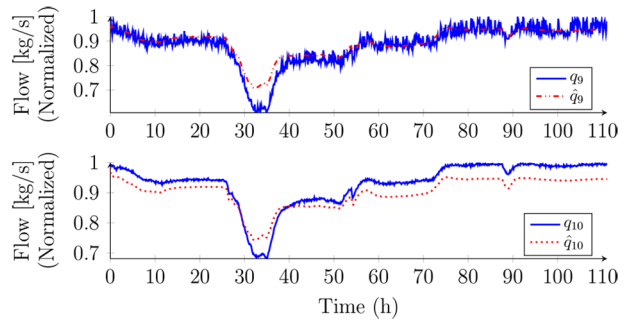

Figure 12. Model validation results for q_9 and q_{10}.

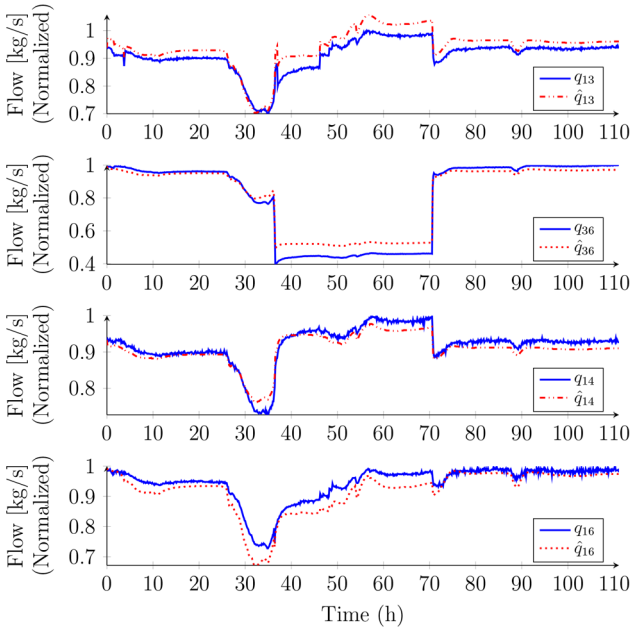

Figure 13. Model validation results for q_{13}, q_{14}, q_{36}, and q_{16}.

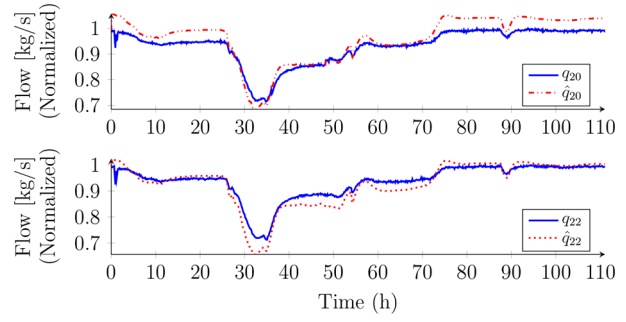

Figure 14. Model validation results for q_{20} and q_{22}.

prediction results in Figure 9 also show a steady-state prediction error after time t = 50 h. The main source of these errors is uncertainties in the choke valve models caused by the scarcity of step test data required to develop accurate models. Model−plant mismatch is always present and can be mitigated, as measurement feedback will be able to correct for the error in control applications.

The low correlation coefficient and NRMSE of the model predictions show that the model can be used for model based control applications. The developed model can also be used to investigate different model based control strategies for natural gas production networks in order to determine the most optimal control system schemes in terms of network pressure stability while maintaining operating constraints at each well.

Table 3. Model Prediction Performance According to Pearson Correlation Coefficient and NRMSE

parameter	$\rho(y, \hat{y})$	NRMSE
P_8	0.9927	0.0304
P_{35}	0.9935	0.0435
P_1	0.9818	0.0366
q_1	0.9910	0.0157
P_2	0.9912	0.0206
q_2	0.9928	0.0487
P_4	0.9920	0.0264
q_4	0.9896	0.0361
P_6	0.9924	0.0291
q_6	0.9909	0.0249
P_9	0.9923	0.0273
q_9	0.9741	0.0433
P_{10}	0.9925	0.0270
q_{10}	0.9921	0.0432
P_{13}	0.9491	0.0297
q_{13}	0.9425	0.0249
P_{36}	0.9714	0.0320
q_{36}	0.9988	0.0508
P_{14}	0.9618	0.0229
q_{14}	0.9522	0.0272
P_{16}	0.9817	0.0268
q_{16}	0.9890	0.0459
P_{20}	0.9915	0.0282
q_{20}	0.9915	0.0455
P_{22}	0.9917	0.0279
q_{22}	0.9910	0.0195

CONCLUSIONS

In this study, SEM was used to develop a model of an industrial natural gas system comprising multiple gas wells and pipelines feeding one consumer. The developed model was shown to produce accurate predictions of the flow rates from each well in the presence of choke valves and consumer demand changes. The developed model was shown to produce an accurate prediction of the consumer battery limit pressure and pressures at the well outlets. The good prediction performance and state-space model form show that the model can be used for model based control applications.

In terms of future work, the developed model can be used to analyze the sensitivity of the model to model parameters such as compressibility, gas composition, temperature, and viscosity in an attempt to simplify the model for reduced computational complexity. A model based controller can be implemented in order to demonstrate the benefit of implementing a model based controller on a natural gas well production network. The model can also be used to evaluate the effect of linearizing the model on the performance of a model based controller. Finally, gas composition tracking can be added to model the scenario where gas from reservoirs with different characteristics are mixed.

AUTHOR INFORMATION

Corresponding Author

Johan Derik le Roux − *Department of Electrical, Electronic and Computer Engineering, University of Pretoria, Pretoria*

https://doi.org/10.1021/acs.iecr.3c00990
Ind. Eng. Chem. Res. 2024, 63, 1461−1473

0002, South Africa; orcid.org/0000-0002-6306-1949; Email: derik.leroux@up.ac.za

Authors

Rudzani Dzedzemane − *Department of Electrical, Electronic and Computer Engineering, University of Pretoria, Pretoria 0002, South Africa*

Andries Johannes Wiid − *Department of Electrical, Electronic and Computer Engineering, University of Pretoria, Pretoria 0002, South Africa*

Ian Keith Craig − *Department of Electrical, Electronic and Computer Engineering, University of Pretoria, Pretoria 0002, South Africa;* orcid.org/0000-0001-7437-3983

Complete contact information is available at: https://pubs.acs.org/10.1021/acs.iecr.3c00990

Notes

The authors declare no competing financial interest.

■ ACKNOWLEDGMENTS

This work is based on the research supported in part by the National Research Foundation of South Africa (Grant Number: 137769).

■ REFERENCES

(1) Wang, X.; Economides, M. *Advanced Natural Gas Engineering*; Gulf Publishing Company, 2009.

(2) Strambo, C.; Burton, J.; Atteridge, A. The end of coal? Planning a "just transition" in South Africa; SEI report. Stockholm Environment Institute: Stockholm, Sweden, 2019. https://www.sei.org/publications/the-end-of-coal-planning-a-just-transition-in-south-africa/ (accessed: 2023−08−30).

(3) International Energy Agency. Electricity Information. https://www.iea.org/data-and-statistics/data-product/electricity-information (accessed: 2023−08−30).

(4) Tordoir, P. Is natural gas the next coal? A framework for utilities and governments to think about the place of natural gas in the energy mix. *Electricity Journal* **2022**, *35*, 107077.

(5) Climate Change Report for the year ended 30 June 2021; Sasol Limited: Secunda, South Africa, 2021. https://sasol.com/sites/default/files/2022-04/Sasol%20Climate%20Change%20Report_2021_22Sep21_0_0.pdf.

(6) The role of gas as a transition fuel in South Africa's path to net-zero. National Business Initiative (NBI): Sandton, South Africa, 2022. https://www.nbi.org.za/climate-pathways-and-a-just-transition-for-south-africa/ (accssed: 2023−08−30).

(7) Guo, B.; Ghalambor, A. *Natural Gas Engineering Handbook*, 2nd ed.; Gulf Publishing Company, 2012.

(8) Bopbekov, D.; Pourafshary, P.; Hazlett, R. Accuracy of droplet models for liquid loading prediction: Analysis of production well parameters. *Journal of Natural Gas Science and Engineering* **2022**, *98*, 104391.

(9) Darby, M. L.; Nikolaou, M. MPC: Current practice and challenges. *Control Engineering Practice* **2012**, *20*, 328−342.

(10) Smith, R. Unsteady-State gas flow into gas wells. *Journal of Petroleum Technology* **1961**, *13*, 1151−1159.

(11) Mikolajková-Alifov, M.; Pettersson, F.; Björklund-Sänkiaho, M.; Saxen, H. A model of optimal gas supply to a set of distributed consumers. *Energies* **2019**, *12*, 351.

(12) Arya, A. K.; Katiyar, R.; Senthil Kumar, P.; Kapoor, A.; Pal, D. B.; Rangasamy, G. A multi-objective model for optimizing hydrogen injected-high pressure natural gas pipeline networks. *Int. J. Hydrogen Energy* **2023**, *48*, 29699−29723.

(13) Mikolajková, M.; Haikarainen, C.; Saxén, H.; Pettersson, F. Optimization of a natural gas distribution network with potential future extensions. *Energy* **2017**, *125*, 848−859.

(14) Mikolajková, M.; Saxén, H.; Pettersson, F. Mixed integer linear programming optimization of gas supply to a local market. *Ind. Eng. Chem. Res.* **2018**, *57*, 5951−5965.

(15) Chaczykowski, M.; Zarodkiewicz, P. Simulation of natural gas quality distribution for pipeline systems. *Energy* **2017**, *134*, 681−698.

(16) Kiuchi, T. An implicit method for transient gas flows in pipe networks. *International Journal of Heat and Fluid Flow* **1994**, *15*, 378−383.

(17) Kessal, M. Simplified numerical simulation of transients in gas networks. *Chem. Eng. Res. Des.* **2000**, *78*, 925−931.

(18) Koo, B. Comparison of finite-volume method and method of characteristics for simulating transient flow in natural-gas pipeline. *Journal of Natural Gas Science and Engineering* **2022**, *98*, 104374.

(19) Bermúdez, A.; Shabani, M. Finite element solution of isothermal gas flow in a network. *J. Comput. Phys.* **2019**, *396*, 616−652.

(20) Zienkiewicz, O.; Taylor, R. *The Finite Element Method*, 5th ed.; Butterworth-Heinemann: Oxford, 2000; Vol. 3, Fluid Mechanics.

(21) Twyman, J. Transient flow analysis using the method of characteristics MOC with five-point interpolation scheme. *Obras y Proyectos* **2018**, 62−70.

(22) Canuto, C.; Hussaini, M.; Quarteroni, A.; Zang, T. *Spectral Methods: Evolution to Complex Geometries and Applications to Fluid Dynamics*; Springer: Berlin, 2007.

(23) Mennemann, J.-F.; Marko, L.; Schmidt, J.; Kemmetmüller, W.; Kugi, A. The spectral element method as an efficient tool for transient simulations of hydraulic systems. *Applied Mathematical Modelling* **2018**, *54*, 627−647.

(24) Wiid, A. J.; Le Roux, J. D.; Craig, I. K. Modelling of methane-rich gas pipeline networks for simulation and control. *Journal of Process Control* **2020**, *92*, 234−245.

(25) Su, H.; Zio, E.; Zhang, Z.-J.; Xiong, C.-Z.; Dai, Q.-S.; Wu, Q.-W.; Zhang, J.-J. Development of an integrated dynamic model for supply security and resilience analysis of natural gas pipeline network systems. *Petroleum Science* **2022**, *19*, 761−773.

(26) Wiid, A. J.; Le Roux, J. D.; Craig, I. K. Pressure buffering control to reduce pollution and improve flow stability in industrial gas headers. *Control Engineering Practice* **2021**, *115*, 104904.

(27) Burchell, J. J.; Le Roux, J. D.; Craig, I. K. Nonlinear model predictive control for improved water recovery and throughput stability for tailings reprocessing. *Control Engineering Practice* **2023**, *131*, 105385.

(28) Muller, C. J.; Craig, I. K.; Ricker, N. L. Modelling, validation, and control of an industrial fuel gas blending system. *Journal of Process Control* **2011**, *21*, 852−860.

(29) Trapp, C.; Casella, F.; Colonna, P. Dynamic Modeling and Validation of a Precombustion CO2 Capture Plant for Control Design. *Ind. Eng. Chem. Res.* **2014**, *53*, 13098−13111.

(30) Walters, M. S.; Lin, Y.-J.; Sachde, D. J.; Edgar, T. F.; Rochelle, G. T. Control Relevant Model of Amine Scrubbing for CO2 Capture from Power Plants. *Ind. Eng. Chem. Res.* **2016**, *55*, 1690−1700.

(31) van de Haar, A.; Trapp, C.; Wellner, K.; de Kler, R.; Schmitz, G.; Colonna, P. Dynamics of Postcombustion CO2 Capture Plants: Modeling, Validation, and Case Study. *Ind. Eng. Chem. Res.* **2017**, *56*, 1810−1822.

(32) Fang, J.; Zeng, Q.; Ai, X.; Chen, Z.; Wen, J. Dynamic optimal energy flow in the integrated natural gas and electrical power systems. *IEEE Transactions on Sustainable Energy* **2018**, *9*, 188−198.

(33) Canuto, C.; Hussaini, M.; Quarteroni, A.; Zang, T. *Spectral Methods: Fundamentals in Single Domains*; Springer: Berlin, 2006.

(34) Ekechukwu, G. K.; Orodu, O. D. Novel mathematical correlation for accurate prediction of gas compressibility factor. *Natural Gas Industry B* **2019**, *6*, 629−638.

(35) Kareem, L. A.; Iwalewa, T. M.; Al-Marhoun, M. New explicit correlation for the compressibility factor of natural gas: linearized z-factor isotherms. *Journal of Petroleum Exploration and Production Technology* **2016**, *6*, 481−492.

(36) Zeghadnia, L.; Robert, J. L.; Achour, B. Explicit solutions for turbulent flow friction factor: A review, assessment and approaches classification. *Ain Shams Engineering Journal* **2019**, *10*, 243−252.
(37) Vatankhah, A. R. Comment on "Gene expression programming analysis of implicit Colebrook−White equation in turbulent flow friction factor calculation. *J. Pet. Sci. Eng.* **2014**, *124*, 402−405.
(38) Yang, X.; Zhang, S.; Zhu, W. A new model for the accurate calculation of natural gas viscosity. *Natural Gas Industry B* **2017**, *4*, 100−105.
(39) Bahadori, A. Estimation of flow coefficient for subsonic natural gas flow through orifice-type chokes using a simple method. *Journal of Natural Gas Science and Engineering* **2012**, *9*, 39−44.
(40) Nejatian, I.; Kanani, M.; Arabloo, M.; Bahadori, A.; Zendehboudi, S. Prediction of natural gas flow through chokes using support vector machine algorithm. *Journal of Natural Gas Science and Engineering* **2014**, *18*, 155−163.
(41) *Flow equations for sizing control valves*; ISA-75.01.01-2007; International Society of Automation: Research Triangle Park, NC, 2007.
(42) Grace, A.; Frawley, P. Experimental parametric equation for the prediction of valve coefficient (Cv) for choke valve trims. *International Journal of Pressure Vessels and Piping* **2011**, *88*, 109−118.
(43) Loegering, M. J.; Milkov, A. V. Geochemistry of petroleum gases and liquids from the Inhassoro, Pande and Temane fields onshore Mozambique. *Geosciences* **2017**, *7*, 33.

https://doi.org/10.1021/acs.iecr.3c00990
Ind. Eng. Chem. Res. 2024, 63, 1461−1473